ISSN 0362-1197, Human Physiology, 2017, Vol. 43, No. 4, pp. 366–376. © Pleiades Publishing, Inc., 2017.
Original Russian Text © V.A. Ponomarev, M.V. Pronina, Yu.D. Kropotov, 2017, published in Fiziologiya Cheloveka, 2017, Vol. 43, No. 4, pp. 13–24.

Dynamics of the EEG Spectral Density in the θ, α, and β Bands in the Visual *Go/NoGo* Task

V. A. Ponomarev*, M. V. Pronina, and Yu. D. Kropotov

Bekhtereva Institute of the Human Brain, Russian Academy of Sciences, St. Petersburg, Russia

**e-mail: valery_ponomarev@mail.ru*

Received December 9, 2016

Abstract—The study was aimed at analyzing event-related desynchronization/synchronization (ERD/ERS) in 19-channel EEGs recorded in 329 healthy subjects in the course of a *Go/NoGo* task. Three methods were tested: reference, current source density (CSD), and group decomposition by independent component analysis (ICA). A comparison of the three data sets showed that the ICA method better reflects the local features of the brain responses in the θ, α, and β ranges. The functional significance of the group ICA components is discussed.

Keywords: electroencephalogram, dynamics of spectral density, *Go/NoGo* task, independent component analysis

DOI: 10.1134/S0362119717040132

INTRODUCTION

Event-related desynchronization/synchronization (ERD/ERS) is thought to provide reliable parameters to estimate the extent of cortical activation associated with the performance of various tasks [1]. Two types of electrical activity, evoked and induced, are recognized in EEG responses. Evoked activity, or event-related potentials (ERPs), are changes in electrical potential that are phase locked to the stimulus or the response, while induced activity is not. ERPs arising in the *Go/NoGo* paradigm have been studied relatively comprehensively [2, 3]. For instance, certain components of the ERPs observed in a visual *Go/NoGo* test with two stimuli have been associated with stimulus categorization and comparison with information stored in working memory; preparation, execution, and suppression of a response; and evaluation of the result [4–6]. Induced EEG activity in the α and β bands has also been shown to include brain response components that are associated with anticipation of a visual stimulus [7, 8], its perception [9–15], preparation to act [16–20], performance of a movement [17, 18, 21–23], and its suppression [17, 18, 20, 24]. Induced EEG activity has mostly been studied in an auditory *Go/NoGo* test [17, 18, 20, 23], while a visual *Go/NoGo* test is rarely used in such studies because substantial desynchronization of α activity associated with presentation of visual stimuli [9] masks other effects.

Potentials recorded from the head surface are superimpositions of fields from several sources. Local cortical activity is usually isolated by converting the EEG to the current source density (CSD) using the surface Laplacian. A limitation of the CSD analysis is that the transform suppresses the signal components with slow spatial changes. Another approach has been proposed relatively recently and is based on a group independent component analysis (gICA) as a means to process the signals from EEG sources [25]. Studies have shown that gICA makes it possible to obtain additional information when comparing the spectral density for various subject groups [25], but it is unclear whether the approach is adequate for analyzing the dynamics of the EEG spectral density.

Our study had two objectives. One was to evaluate whether a signal analysis with the gICA model is adequate and informative for studying the dynamics of the EEG spectral density. The second objective was to study the dynamics of brain processes that occur in the *Go/NoGo* test and are reflected in induced EEG activity.

METHODS

A total of 329 healthy subjects (including 184 females) aged 20–50 years participated in the study. The study was carried out in accordance with the Declaration of Helsinki for research involving human subjects. All subjects were informed about the study procedure and gave their written consent to participation.

In the psychological test to be performed by the subjects, visual stimuli of three categories, that is, images of animals (A), plants (P), and humans (H), 20 images in each category, were presented on a computer monitor. Images of approximately 3.8° in angu-

lar dimensions were presented at the center of the monitor against a white background. The white background was displayed between stimulus presentations. Image presentation was not accompanied by screen blinking. A test included 400 trials. The total test duration was 21 min. A pair of stimuli was presented in each trial. A stimulus was presented for 100 ms, the interval between two stimuli in a pair was 1000 ms, and the interval between the starting points of stimulus pairs was 3100 ms. All trials were divided into four equal groups depending on the combination of stimuli in a pair. The following combinations were used: A–A, A–P, P–P, and P–H. In the case of the A–A and P–P pairs, the two images of animals or plants that were presented in a pair were identical. In the case of the P–H pairs, the second stimulus was presented simultaneously with a sound signal (the sound pressure level was approximately 70 dB). Sound signals were random sequences of rapidly changing tones with a duration of 20 ms and frequencies of 500, 1000, 1500, 2000, and 2500 Hz. The test was divided into blocks of 100 trials each. Each block included presentation of 15 different images, including five images of each category, which were combined to obtain 20 pairs of stimuli. Different images were used in different blocks. Trials were presented in a quasirandom order. The Psytask program was employed in stimulus presentation. The subject had to press a button with his or her right hand after the presentation of the A–A pair, acting as fast and accurately as possible. When the task was performed incorrectly, the trial was excluded from the analysis. The subject was trained using several tens of trials prior to starting the test. One or a few short pauses (1–2 min each) were made during the test to allow the subject to rest.

The EEG was recorded using a Mitsar-EEG computerized electroencephalograph. The electrodes were positioned according to the international 10–20 system at the sites Fp_1, Fp_2, F_7, F_3, Fz, F_4, F_8, T_3, C_3, Cz, C_4, T_4, T_5, P_3, Pz, P_4, T_6, O_1, and O_2. Linked earlobe electrodes were used as a reference, and the Fpz electrode was used as a ground. The electrode impedance did not exceed 5 kΩ. The sampling rate was 250 Hz. The settings for the high-pass and low-pass filters were 0.53 ($\tau = 0.3$ s) and 50 Hz, respectively. A digital notch filter with a reject band of 45–55 Hz was used to remove electromagnetic power line interferences.

The WinEEG program was employed in data processing. Eye blink-related artifacts were eliminated by bringing the corresponding EEG independent components to zero [26, 27]. Trials with artifact-containing EEGs were excluded from further analysis. A EEG recording was identified as containing artifacts when there were (1) potentials of more than 50 μV for the Fp_1 and Fp_2 and more than 100 μV for the other electrodes, (2) slow waves with amplitudes exceeding 50 μV in a range of 0.53–1 Hz, or (3) fast signal oscillations with an amplitude of more than 35 μV in a range of 20–35 Hz. The limits were selected empirically by repeating the data processing procedure with different parameters and evaluating the results visually.

The spectral density dynamics was calculated for the initial EEG, its CSD derivative, and gICA signals [25]. Computations were performed by two methods, with and without subtracting averaged ERPs from the corresponding individual trials. The ERP effect on the spectral density dynamics was partly eliminated in the former case. Six variants of evaluating the dynamics of spectral density were examined as a result and were compared with each other.

The CSD was estimated using an algorithm that utilizes spherical splines to interpolate the potential distribution [28] and produces adequate results when analyzing the EEGs obtained with relatively low-density scalp locations of electrodes [29].

To estimate the group independent components of the EEG, we used the linear instant mixture model $x(t) = As(t)$, where $x(t) = \{x_1(t),\ldots,x_N(t)\}^T$ is the original EEG signal, N is the number of electrodes, $t = 1,\ldots,T$ is the time, and $s(t) = \{s_1(t),\ldots,s_M(t)\}^T$ is the number of signals from electrical field sources, M is the number of sources, and A is the mixing matrix $N \times M$. The source topography is described by the column-vector $\{a_{1j},\cdots,a_{Nj}\}^T$, which includes coefficients describing the effect of the j-th source on the electrical potentials of all electrodes. The mixing matrix A was evaluated simultaneously for all EEG recordings, which were preliminarily subjected to band filtration of the original signal with Kaiser digital filters of the order 512 with a finite impulsed response and a bandpass range of 4–40 Hz and were combined to produce one time series. Evaluation of the mixing matrix A was performed with a natural gradient iterative algorithm [30], wherein the function $\varphi_i(y_i)$ took the form

$$\varphi_i(y_i) = \left(\ln r_i'(y_i)\right)', \quad \text{where} \quad r_i(y_i) = 1\Big/\left(1 + e^{-y_i}\right).$$

This algorithm modification is often referred as Infomax in the literature. We used the algorithm implementation created in the C++ language and incorporated in the WinEEG program; the implementation was identical to the runica() procedure of the EEGLAB package [31].

The optimal source number M was estimated using the theoretical Akaike information criterion (AIC) [32]. The reliability of the models was checked using tests with random sampling of two nonoverlapping epochs from a EEG recording, random sampling of a sample subset from a EEG recording, and random division of the total set of EEG recording into halves [25]. The testing results were similar to those reported previously [25]. To avoid repetitions, we mention here only that the optimal source number was 19 and that

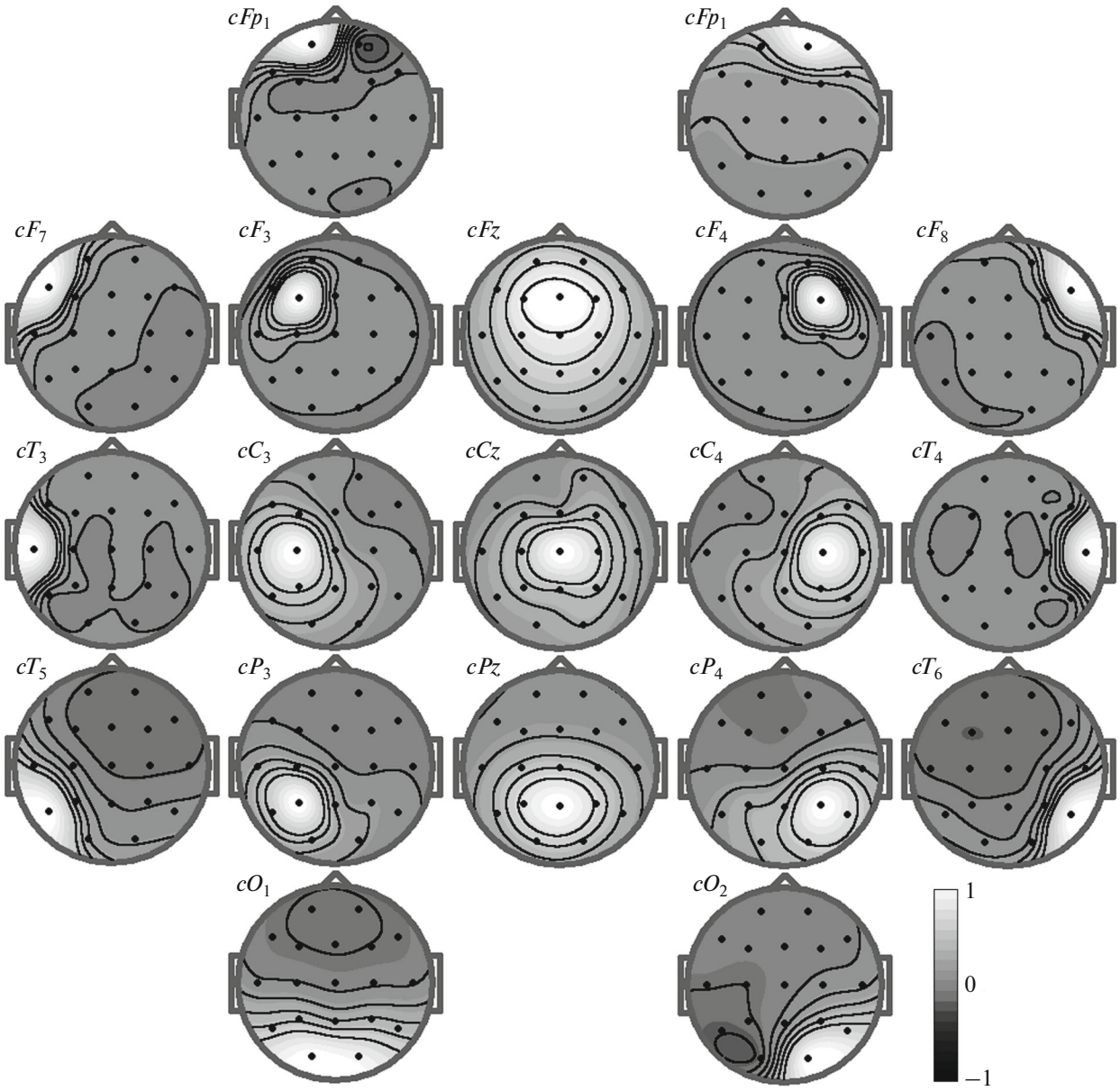

Fig. 1. Source topographies in the gICA model.

the evaluation of the mixing matrix A was highly reliable because more than 300 EEG recordings with duration of approximately 20 min were used for the analysis. The resulting source topography estimates are shown in Fig. 1.

The spectral density dynamics was calculated separately for each subject, each electrode, and each of the four trial groups (A–A, A–P, P–P, and P–H). A convolution of the original signal $x_i(t)$ and the Morlet wavelet was obtained as $w_i(f,t) = \int_{-\infty}^{\infty} x_i(t')\psi(t'-t)dt'$, where $\psi(t) = \frac{1}{\sqrt{\sigma\sqrt{\pi}}}\exp(-i2\pi ft)\exp\left(-\frac{t^2}{2\sigma^2}\right)$, f is the central frequency of the wavelet, σ is selected so that $2\pi\sigma f = 5$ for all f values [33]. The wavelet transform was performed for several f values ranging from 2 to 30 Hz with a 1-Hz step. The spectral density was obtained as $S_i(f,t) = |w_i(f,t)|^2$, and averaged over trials of one group. When calculating the spectral density dynamics for the interval between the first and second stimuli, averaging was performed over the trials that included images of the same category (hereafter referred to as A+ and P–). The spectral density dynamics was averaged over all subjects, and difference curves (A–A)–(A–P), (P–P)–(P–H), and A+ – P– were computed. To obtain a graphic representation, the spectral density was normalized as

$\overline{S}_i(f,t) = \left(\overline{S}_i(f,t) - \overline{S}_i^{BG}(f)\right)\Big/\overline{S}_i^{BG}(f)$, where the index BG means averaging over the interval preceding the first stimulus.

Pairwise differences between groups of trials were tested for significance by Student's *t* test for dependent samples. Logarithm transformation of $S_i(f,t)$ values was applied for each subject separately for normalization when the spectral density was analyzed. Significance testing of differences was performed separately for each pair of conditions, each wavelet central frequency *f*, and each time moment *t*; i.e., several tens of thousands of statistical comparisons were performed. A correction for multiple comparisons was therefore necessary. The Bonferroni correction yields excessively conservative estimates because a substantial autocorrelation is characteristic of the spectral power dynamics. A statistical significance threshold was therefore selected empirically. In particular, it turned out that differences significant at $p < 10^{-4}$ were not observed in the interval preceding the first stimulus and the interval between the first and second stimuli when comparisons were performed for the conditions A–A and A–P or P–P and P–H. However, the higher significance level $p < 10^{-5}$ was chosen to reduce the probability of false positive results.

RESULTS

Comparisons showed that similar patterns of the spectral density dynamics were obtained for the original EEG, CSD, and signals in the gICA model. The frequency ranges and the spatial locations and latencies of peaks of the most distinct effects were approximately the same. However, the spatial pattern of changes in power was more blurred in the case of the original EEG than in the cases of CSD and signals in the gICA model. The spectral density dynamics obtained for CSD and signals in the gICA model were similar, but not identical. Local effects in the region of the *Fz* electrode were greater with CSD. Other local effects were greater in the case of the gICA model. The most distinct changes in power were observed only for some frequency ranges, which corresponded to wavelet central frequencies *f* of 5, 10, 15, 17, and 20 Hz. Each of these frequency ranges was examined separately in further analysis.

In the θ band ($f = 5$ Hz), the power of the signal increased after presentation of a stimulus; the peak amplitude and latency of the signal depended on the trial type and the location. Peak latency varied from 150 to 800 ms. In addition, decreases in signal power in the A+ and A–A trials occurred later and were lower (usually lower than 20%) in the posterior regions. The magnitude of these responses depended on whether group-averaged ERPs were subtracted from individual samples.

The dynamics of spectral density in the α band ($f =$ 10 Hz) is considered below for signals of the gICA model, wherein local effects were greater as compared with the original EEG and CSD. Examples of the most distinct responses are shown in Fig. 2; the corresponding difference curves and statistical significance of differences are shown in Fig. 3.

Interval between the first and second stimuli in the trials A+ and P–. (1) In the case of the cT_5, cP_3, cPz, cP_4, cT_6, cO_1, and cO_2 sources, signal power decreased within the first 300 ms after stimulus presentation and was independent of the trial type. The significance of this response is characterized in Fig. 3 (component *A*1). Then the signal power increased at a rate that was greater in P– than in A+ trials. A difference in signal power (Fig. 3, component *A*4) became detectable approximately 400 ms after the first stimulus and reached its maximum prior to the second stimulus. The responses were maximal in signals from the cO_1 and cO_2 sources. (2) In the case of the cC_3 source, the signal power observed in A+ trials started to decrease approximately 300–400 ms after the first stimulus, reached its minimum at 600 ms, and remained unchanged up to the presentation of the second stimulus. In the case of P– trials, changes in signal power were not observed. The difference is seen from the corresponding difference curve (Fig. 3, component *A*5). (3) In the case of the cF_7 source, a relative increase in signal power was observed prior to the presentation of the second stimulus in trials A+ compared with trials P– with a maximum of ~300 ms prior to the second stimulus (Fig. 3, component A6). Note that this response was observed only in signals of the gICA model and was undetectable in the power dynamics obtained for the original EEG and CSD.

Interval after the second stimulus in the trials A–A and A–P. (1) In the case of the cO_1 and cO_2 sources, the signal power reached its minimum approximately 300–400 ms after the stimulus presentation and then increased. The shape of these changes was much the same in the A–A and A–P trials. (2) In the case of the cC_3 and cC_4 sources, the signal power in the A–A trials reached its minimum approximately 600–700 ms after the presentation of the second stimulus and then increased. A lower decrease in power was observed in the A–P trials. Difference curves (Fig. 3, component *A*2) showed a distinct difference in signal power between the A–A and A–P trials. Other sources also displayed differences in signal power between the A–A and A–P trials, but the differences were lower.

Interval after the second stimulus in the trials P–P and P–H. A decrease in signal power was observed for the cT_5, cP_3, cPz, cP_4, cT_6, cO_1, and cO_2 sources. Decreases observed in the P–H trials were greater than in the P–P trials. The greatest difference was detected for signals from the cPz source with a peak latency of ~300–400 ms (Fig. 3, component *A*3).

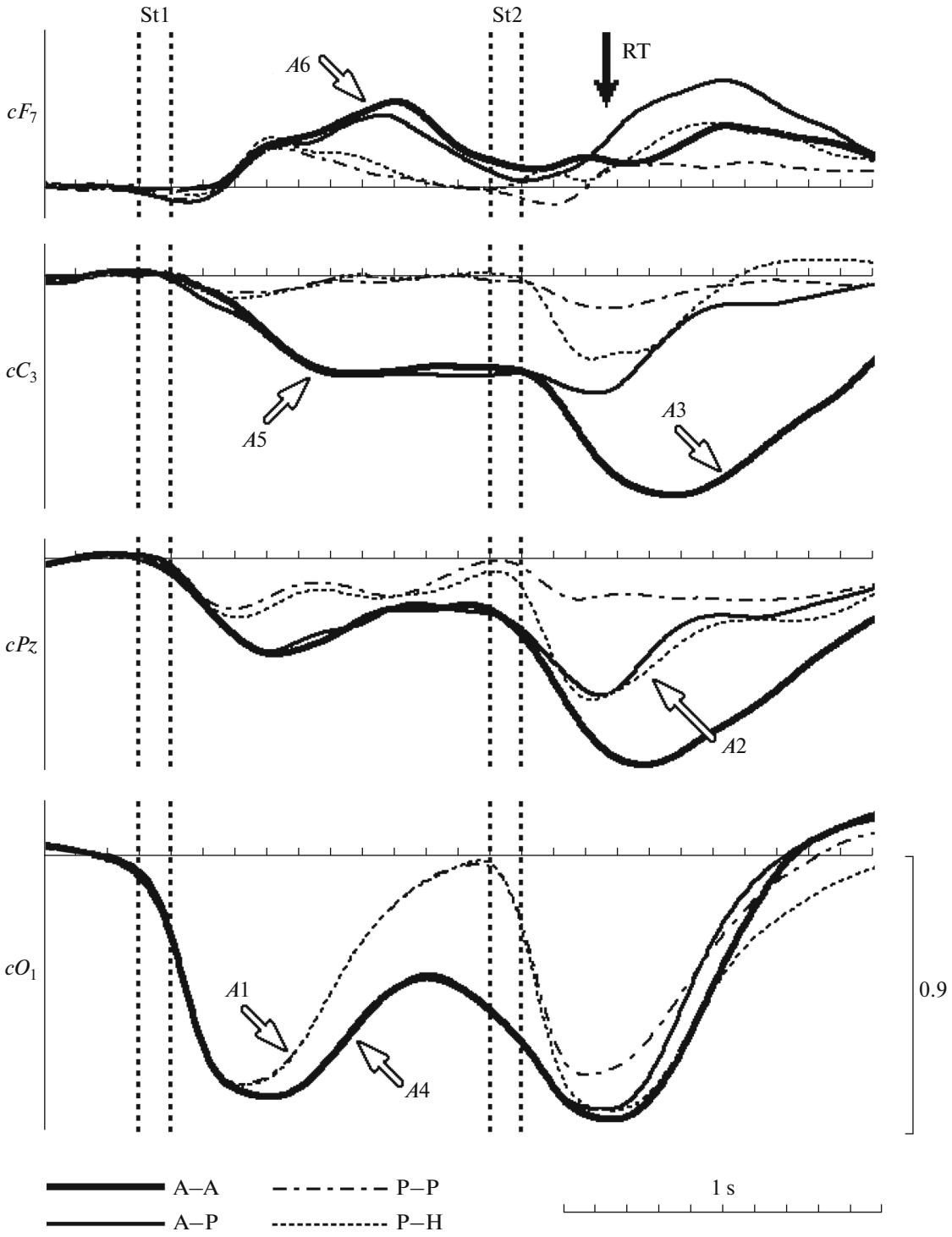

Fig. 2. Dynamics of spectral density in the α band. *A*1–*A*6, components of α-activity responses (see Fig. 3). Abscissa, time; ordinate, normalized deviation of power density from its mean value observed in the time interval preceding the first stimulus. Start and end points of the stimuli are shown with vertical dashed lines. St1 and St2 are the first and second stimuli in a trial, respectively. RT is the response time.

In the β band, the greatest changes in spectral density were observed for lower-frequency oscillations ($f = 15$ Hz) in the frontal regions and higher-frequency oscillations ($f = 17$ or 20 Hz) in the central and posterior regions. Examples of the most distinct responses are shown in Fig. 4; the corresponding difference curves and statistical significance of differences are shown in Fig. 5. In the frontal regions, the greatest

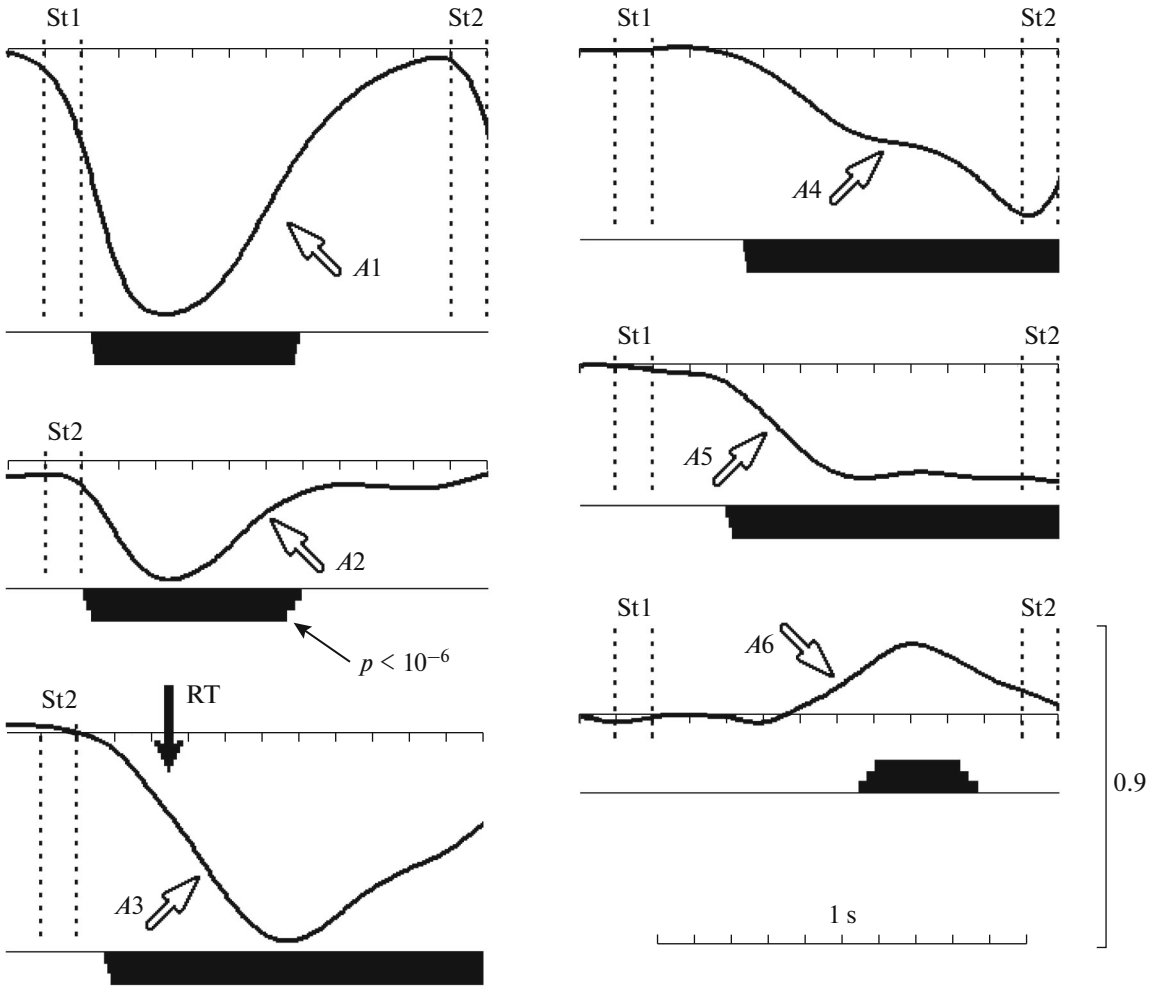

Fig. 3. Components of the α-activity responses. *A*1, dynamics of spectral density after the first stimulus in the P– trials. The other plots show the difference curves: *A*2, (P–H)–(P–P); *A*3, (A–A)–(A–P); *A*4–*A*6, A+ –P–. Bars at the bottom of a plot characterize the statistical significance of the respective effects: a short bar, $p < 10^{-4}$; a medium bar, $p < 10^{-5}$; and a long bar, $p < 10^{-6}$. Other designations are as in Fig. 2.

changes were observed in the CSD analysis for the *Fz* electrode. The corresponding plots are therefore shown in Figs. 4 and 5. Other responses were better seen in signals of the gICA model.

Interval between the first and second stimuli in the trials A+ and P–. (1) The cT_5, cP_3, cPz, cP_4, cT_6, cO_1, and cO_2 sources showed a decrease in signal power with a peak at ~200–300 ms; the decrease did not depend on the trial type. The magnitude of the response was the highest in the lower-frequency range ($f = 15$ Hz) for the cO_1 and cO_2 sources. Then the signal power increased, reached its maximum, and started to decrease. The power increase rate in the P– trials was higher than in the A+ trials. The maximum value was again observed for the cO_1 and cO_2 sources, but in another frequency range ($f = 17$ Hz). The curves characterizing the difference in signal power between the conditions A+ and P– were much the same in shape with all sources (Fig. 5, component *B*3). A difference became detectable at 300–400 ms and reached its maximum in the range ~550–600 ms. Afterwards, the difference decreased up to 800 ms and increased again until the second stimulus was presented. (2) The cC_3 source showed a decrease in signal power in the A+ trials; a peak was at ~600 ms; the decrease started 300–400 ms after the presentation of the first stimulus and continued until the second stimulus was presented. In the P– trials, decreases in power were lower. The difference in responses is shown in Fig. 5 (component *B*5). (3) In the case of CSD, the *Fz* source showed an increase in signal power in the β band, especially for $f_0 = 15$ Hz. The magnitude of the effect was greater in the A+ trials; the peak latency was ~600 ms (Figs. 4, 5; component *B*1).

Interval after the second stimulus in the trials A–A and A–P. (1) The cT_5, cT_6, cO_1, and cO_2 sources showed a decrease in signal power with a peak at ~200–

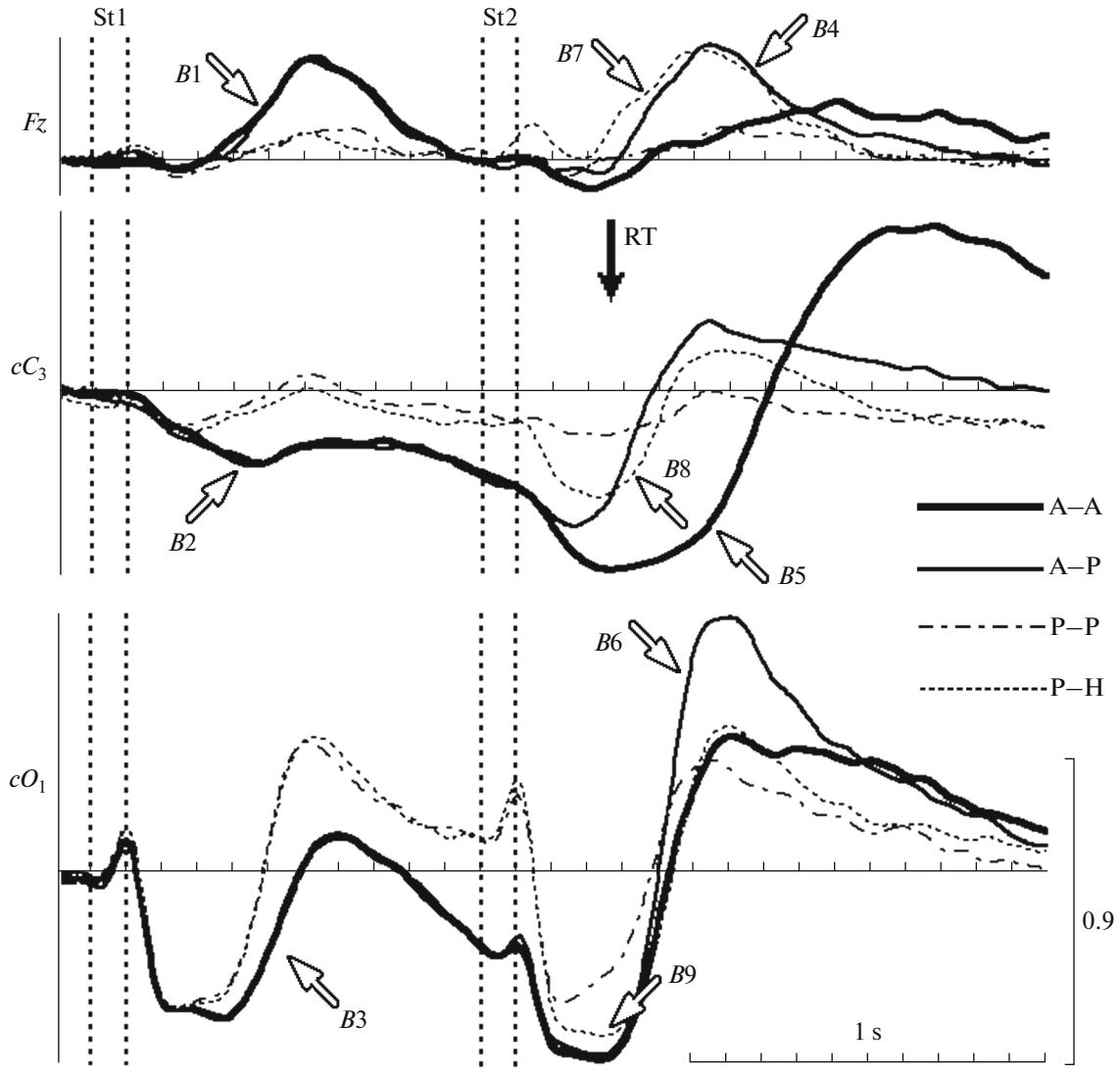

Fig. 4. Dynamics of spectral density in the β band. *B*1–*B*9, components of the β-activity responses (see Fig. 5). Designations are as in Fig. 2.

300 ms. The greatest response was observed for the cO_1 and cO_2 sources in the lower-frequency range (f = 15 Hz). No difference in signal power between the A–A and A–P trials was observed for the first 400 ms. Then a rapid increase in signal power with a maximum at ~600–700 ms was observed in the A–P trials, while the effect was lower in the A–A trials. The difference in power dynamics between the A–A and A–P conditions was the greatest in the time interval 600–700 ms and the frequency range corresponding to f = 17 Hz (Fig. 5, component *B*6). (2) The cC_3, cCz, and cC_4 sources similarly showed a decrease in signal power, and then the signal power increased (Fig. 4). However, the effects were of greater amplitude and longer duration in the A–A trials compared with A–P trials. As a result, the difference curve (Fig. 5, component *B*5) had two peaks, which were maximal in magnitude in the case of signals from the cC_3 source. The latencies of the peaks were 500–600 and 1200–1300 ms, respectively. In addition, the first peak was better seen in the frequency ranges corresponding to f = 15 Hz and f = 17 Hz, while the second peak was greater at f = 20 Hz. The signal power dynamics of the cP_3, cPz, and cP_4 sources were similar within the first 800–900 ms. However, these sources differed from the cC_3, cCz, and cC_4 sources in that a late increase in signal power in the interval 900–1400 ms was not observed in the A–A trials. (3) In the case of CSD, the *Fz* source showed a relatively slow increase in power in the interval 500–1400 ms in the A–A trials. The magnitude and rate of the increase in power in the A–P trials were greater. The difference curves (Fig. 5, component 4) showed that the difference was maximal at ~600 ms and was especially distinct for f = 15 Hz.

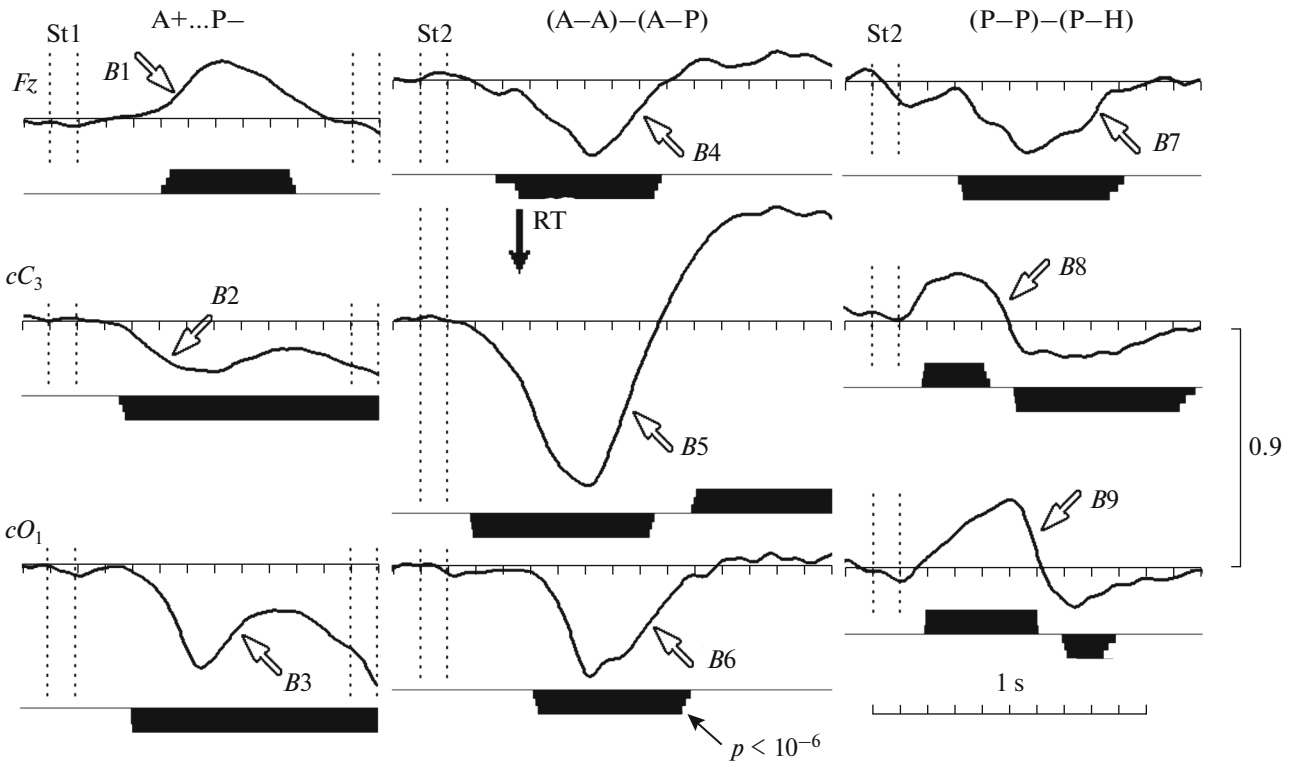

Fig. 5. Components of the β-activity responses. *B*1–*B*3, *B*4–*B*6, and *B*7–*B*9 are the difference curves for A+ – P–, (A–A)–(A–P), and (P–P)–(P–H), respectively. Designations are as in Fig. 3.

Interval after the second stimulus in the trials P–P and P–H. (1) The dynamics of signal power of the cC_3, cCz, cC_4, cT_5, cP_3, cPz, cP_4, cT_6, cO_1, and cO_2 sources were characterized by a decrease in signal power in the time interval 200–600 ms (with a peak at ~300–400 ms), then the signal power increased. A decrease in signal power was especially high in the case of the cO_1 and cO_2 sources at f = 15 Hz and was relatively greater in magnitude in the P–H trials compared with the P–P trials. A subsequent increase in power had a peak latency in the interval 700–800 ms and was again greater for the cO_1 and cO_2 sources in the P–H trials, but at f = 17 Hz. The differences in these responses between the P–P and P–H trials are shown in Fig. 5 (components *B*8 and *B*9). (2) In the case of CSD, the *Fz* source showed an increase in power in the interval 500–900 ms with a peak latency of ~700 ms. The peak amplitude was greater in the P–H trials (Figs. 4, 5; component *B*7). The effect was the greatest in the case of f = 15 Hz.

DISCUSSION

The gICA model provides an efficient tool for studying the brain mechanisms. The model adequately describes the properties known signals for various brain regions. Local features of these signals are better seen in the gICA model compared with conventional methods. The gICA model made it possible to detect several characteristics that are difficult, if possible at all, to observe for brain processes with conventional methods. For instance, an increase in the spectral density of α-band signals from the left frontal area of the cortex during preparation to perceiving visual stimuli and performing a motor response is clearly seen with signals of the gICA model, but is undetectable in the original EEG or CSD.

Consider now the EEG responses observed in the visual *Go/NoGo* test.

In the θ band, the spectral density of signals increases after stimulus presentation. The magnitude of the effect depends on whether the ERP is subtracted from the EEG epochs corresponding to individual trials and is greater when the subtraction is not performed. However, ERP subtraction does not ensure a total elimination of evoked activity because its shape varies among trials. Hence, the dependence of spectral power on the type of stimuli and the type of responsive action may be associated with both changes in amplitude of oscillations in the θ band and changes in ERP shape; i.e., its unique interpretation is impossible (for discussion, see [34]).

Several components are possible to isolate in the dynamics of spectral density of α-band signals (Fig. 3).

Component *A*1, which is observed after the first and second stimuli and is especially distinct in the posterior regions, describes the well-known phenomenon, that is, desynchronization of the occipital α-rhythm in response to presentation of a visual stimulus [9]. Component *A*2 describes the difference in spectral density dynamics observed between the P–H and P–P trials for the period after presentation of the second stimulus. This desynchronization of the α rhythm in the parietal regions cannot be directly related to the perception of auditory stimuli [35–37]. It is possible that the effect is related to the orientation response [38–40] or reflects multimodal integration processes. Component *A*3, which was observed after presentation of the second stimulus in the A–A trials and was the greatest in the central cortical regions close to the C_3 and C_4 electrodes, describes the known response of μ-rhythm desynchronization associated with voluntary movements [21] or movements induced by external events [17, 18]. Component *A*4, which was observed in the A+ trials and was especially clearly seen in the posterior regions, describes the known response of occipital α-rhythm desynchronization associated with expectation of a stimulus [7, 8]. Component *A*5, which was observed in the A+ trials and was the greatest in the central cortical regions contralateral to the hand used to press the button, describes the known response of μ-rhythm desynchronization that occurs prior to starting the movement triggered by imperative stimulus [17, 18, 20] and reflects the preparation to a subsequent motor response. Component *A*6, which was observed in the A+ trials, is an increase in power and is especially high in the left frontal regions of the cortex. This effect is undetectable in the original EEG and CSD, but can be isolated using the gICA model. Sources of this signal are in the frontal cortical regions close to the Broca's area of the left hemisphere. The same regions show a decrease in EEG power in the α band during speech activity [41–46]. It is therefore possible that component *A*6 reflects the processes of speech activity inhibition during expectation of a stimulus and preparation for a movement.

In the β band, we observed three patterns of spectral density dynamics (Fig. 4), which were characteristic of the frontal, centro-parietal, and occipito-temporal regions of the brain.

In the centro-parietal regions (Fig. 4b), a decrease in β-rhythm power of the temporal regions (Fig. 4b) was observed prior to the movement in the A+ trials. A similar phenomenon has been observed during voluntary movements [16] and after a warning stimulus [19]. The effect is presumably related to the preparation to movements. In addition, the β-rhythm power decreased and then increased in the A–A trials. A similar phenomenon has been during movements or imagination of movements [22]. A decrease in power is thought to reflect activation of the motor cortex, and a subsequent increase is associated with inhibition following excitation (rebound). Finally, a decrease and an increase in β-rhythm power were observed in the A–P trials. The phenomena have already been described [17, 18, 24] and presumably reflect the processes of making a decision to cancel the prepared movement.

In the occipital and temporal regions, the β-rhythm power increased after stimulus presentation and increased afterwards (Fig. 4c). A decrease in β-rhythm power is presumably associated with perception of visual images and attention processes [10–12]. A later increase in β-rhythm power, which occurs in the interval 500–1000 ms, is poorly understood. This phenomenon is seen in figures and diagrams in almost all of the studies cited above and has been assumed to reflect inhibition of the visual areas during movement performance in some of them [10, 11]. Our findings indicate that the phenomenon is observed even when a movement is not performed. The increase in power of the occipital β-rhythm is likely to reflect inhibition of the visual cortex after its excitation.

In the frontal regions, the β-rhythm power increased after the first and the second stimuli (Fig. 4a). A similar phenomenon has already been reported [17, 18, 20] and is probably more complex than assumed earlier. This β-rhythm response is presumably associated with making a decision about the subsequent action [17, 18]. This assumption can be accepted, but with certain clarifications. First, an action should be considered in a broad sense of the word rather than limited to a movement or its cancelation. Second, a similar late EEG response was observed in the A–A trials after a movement started, when a decision had already been made. Hence, this response seems to reflect inhibition of the frontal cortex after the decision is made rather than the decision-making process itself.

CONCLUSIONS

Our study of the dynamics of EEG spectral density showed that many processes take place in the human brain in the course of a visual *Go/NoGo* test and are reflected in various components of induced EEG activity. The analysis of large data sets with modern methods made it possible to describe the dynamics of the processes in more detail. However, many questions remain open. In particular, the functional significance is unclear for several processes that occur in the brain during stimulus perception and a subsequent response. Further studies are necessary for clarifying these issues.

ACKNOWLEDGMENTS

We are grateful to A. Müller (Children's Research Center, Chur, Switzerland) for EEG recordings in the *Go/NoGo* test.

This work was supported by the Russian Science Foundation (project no. 16-15-10213).

REFERENCES

1. Pfurtscheller, G., *The cortical activation model* (CAM), *Prog. Brain Res.*, 2006, vol. 159, p. 19.
2. Folstein, J.R. and Van Petten, C., Influence of cognitive control and mismatch on the N2 component of the ERP: A review, *Psychophysiology*, 2008, vol. 45, no. 1, p. 152.
3. Polich, J., Neuropsychology of P300, in *The Oxford handbook of Event-Related Potential Components*, Luck, S.J. and Kappenman, E.S., Eds., Oxford: Oxford Univ. Press, 2012, p. 159.
4. Ponomarev, V.A. and Kropotov, Yu.D., Improving source localization of event-related potentials in the GO/NOGO task by modeling their cross-covariance structure, *Hum. Physiol.*, 2013, vol. 39, no. 1, p. 27.
5. Kropotov, J.D. and Ponomarev, V.A., Differentiation of neuronal operations in latent components of event-related potentials in delayed match-to-sample tasks, *Psychophysiology*, 2015, vol. 52, no. 6, p. 826.
6. Kropotov, J., Ponomarev, V., Tereshchenko, E.P., et al., Effect of aging on ERP components of cognitive control, *Front. Aging Neurosci.*, 2016, vol. 8, p. 69.
7. Bastiaansen, M.C. and Brunia, C.H., Anticipatory attention: An event- related desynchronization approach, *Int. J. Psychophysiol.*, 2001, vol. 43, no. 1, p. 91.
8. Deiber, M.P., Sallard, E., Ludwig, C., et al., EEG alpha activity reflects motor preparation rather than the mode of action selection, *Front. Integr. Neurosci.*, 2012, vol. 6, p. 59.
9. Pfurtscheller, G., Neuper, C., and Mohl, W., Event-related desynchronization (ERD) during visual processing, *Int. J. Psychophysiol.*, 1994, vol. 16, nos. 2–3, p. 147.
10. Vázquez Marrufo, M., Vaquero, E., Cardoso, M.J., and Gomez, C.M., Temporal evolution of alpha and beta bands during visual spatial attention, *Brain Res. Cognit. Brain Res.*, 2001, vol. 12, no. 2, p. 315.
11. Pesonen, M., Hämäläinen, H., and Krause, C.M., Brain oscillatory 4-30 Hz responses during a visual *n*-back memory task with varying memory load, *Brain Res.*, 2007, vol. 1138, p. 171.
12. Mishra, J., Martínez, A., Schroeder, C.E., and Hillyard, S.A., Spatial attention boosts short- latency neural responses in human visual cortex, *NeuroImage*, 2012, vol. 59, no. 2, p. 1968.
13. Zhang, D., Wang, L., Luo, Y., and Luo, Y., Individual differences in detecting rapidly presented fearful faces, *PLoS One*, 2012, vol. 7, no. 11, e49517.
14. Van der Lubbe, R.H. and Utzerath, C., Lateralized power spectra of the EEG as an index of visuospatial attention, *Adv. Cognit. Psychol.*, 2013, vol. 9, no. 4, p. 184.
15. Van der Lubbe, R.H., Bundt, C., and Abrahamse, E.L., Internal and external spatial attention examined with lateralized EEG power spectra, *Brain Res.*, 2014, vol. 1583, p. 179.
16. Stancák, A. and Pfurtscheller, G., Event-related desynchronisation of central beta-rhythms during brisk and slow self-paced finger movements of dominant and nondominant hand, *Cognit. Brain Res.*, 1996, vol. 4, no. 3, p. 171.
17. Alegre, M., Gurtubay, I.G., Labarga, A., et al., Frontal and central oscillatory changes related to different aspects of the motor process: A study in go/no-go paradigms, *Exp. Brain Res.*, 2004, vol. 159, no. 1, p. 14.
18. Alegre, M., Imirizaldu, L., Valencia, M., et al., Alpha and beta changes in cortical oscillatory activity in a *Go/NoGo* randomly-delayed-response choice reaction time paradigm, *Clin. Neurophysiol.*, 2006, vol. 117, no. 1, p. 16.
19. Doyle, L.M.F., Yarrow, K., and Brown, P., Lateralization of event-related beta desynchronization in the EEG during pre-cued reaction time tasks, *Clin. Neurophysiol.*, 2005, vol. 116, no. 8, p. 1879.
20. Funderud, I., Lindgren, M., Løvstad, M., et al., Differential Go/NoGo activity in both contingent negative variation and spectral power, *PLoS One*, 2012, vol. 7, no. 10, e48504.
21. Babiloni, C., Carducci, F., Cincotti, F., et al., Human movement- related potentials vs desynchronization of EEG alpha rhythm: A highresolution EEG study, *NeuroImage*, 1999, vol. 10, no. 6, p. 658.
22. Pfurtscheller, G., Neuper, C., and Brunner, C., and da Silva, F.H., Beta rebound after different types of motor imagery in man, *Neurosci. Lett.*, 2005, vol. 378, no. 3, p. 156.
23. Schmiedt-Fehr, C., Mathes, B., Kedilaya, S., et al., Aging differentially affects alpha and beta sensorimotor rhythms in a go/nogo task, *Clin. Neurophysiol.*, 2016, vol. 127, no. 10, p. 3234.
24. Solis-Escalante, T., Müller-Putz, G.R., Pfurtscheller, G., and Neuper, C., Cue-induced beta rebound during withholding of overt and covert foot movement, *Clin. Neurophysiol.*, 2012, vol. 123, no. 6, p. 1182.
25. Ponomarev, V.A., Mueller, A., Candrian, G., et al., Group independent component analysis (gICA) and current source density (CSD) in the study of EEG in ADHD adult, *Clin. Neurophysiol.*, 2014, vol. 125, no. 1, p. 83.
26. Vigário, R.N., Extraction of ocular artefacts from EEG using independent component analysis, *Electroencephalogr. Clin. Neurophysiol.*, 1997, vol. 103, no. 3, p. 395.
27. Tereshchenko, E.P., Ponomarev, V.A., Kropotov, Yu.D., and Müller, A., Comparative efficiencies of different methods for removing blink artifacts in analyzing quantitative electroencephalogram and event-related potentials, *Hum. Physiol.*, 2009, vol. 35, no. 2, p. 124.
28. Perrin, F., Pernier, J., Bertrand, O., and Echallier, J.F., Spherical splines for scalp potential and current density mapping, *Electroencephalogr. Clin. Neurophysiol.*, 1989, vol. 72, no. 2, p. 184.
29. Kayser, J. and Tenke, C.E., Principal components analysis of Laplacian waveforms as a generic method for identifying ERP generator patterns: II. Adequacy of low- density estimates, *Clin. Neurophysiol.*, 2006, vol. 117, no. 2, p. 369.

30. Amari, S., Natural gradient works efficiently in learning, *Neural Comput.*, 1998, vol. 10, no. 2, p. 251.
31. Delorme, A. and Makeig, S., EEGLAB: An open source toolbox for analysis of single-trial EEG dynamics including independent component analysis, *J. Neurosci. Methods*, 2004, vol. 134, no. 1, p. 9.
32. Akaike, H., A new look at statistical model identification, *IEEE Trans. Autom. Control*, vol. 19, no. 6, p. 716.
33. Tallon-Baudry, C., Kreiter, A., and Bertrand, O., Sustained and transient oscillatory responses in the gamma and beta bands in a visual short-term memory task in humans, *Visual Neurosci.*, 1999, vol. 16, no. 3, p. 449.
34. Bastiaansen, M., Mazaheri, A., and Jensen, O., Beyond ERP's: Oscillatory neuronal dynamics, in *The Oxford Handbook of Event- Related Potential Components*, Luck, S.J. and Kappenman, E.S., Eds., Oxford: Oxford Univ. Press, 2012, p. 31.
35. Krause, C.M., Lang, H.A., Laine, M., et al., Event-related desynchronization evoked by auditory stimuli, *Brain Topogr.*, 1994, vol. 7, no. 2, p. 107.
36. Hartmann, T., Schlee, W., and Weisz, N., It's only in your head: Expectancy of aversive auditory stimulation modulates stimulus-induced auditory cortical alpha desynchronization, *NeuroImage*, 2012, vol. 60, no. 1, p. 170.
37. Strauß, A., Wöstmann, M., and Obleser, J., Cortical alpha oscillations as a tool for auditory selective inhibition, *Front. Hum. Neurosci.*, 2014, vol. 8, p. 350.
38. Höller, Y., Kronbichler, M., Bergmann, J., et al., EEG frequency analysis of responses to the own-name stimulus, *Clin. Neurophysiol.*, 2011, vol. 122, no. 1, p. 99.
39. Ruby, P., Blochet, C., Eichenlaub, J.-B., et al., Alpha reactivity to complex sounds differs during rem sleep and wakefulness, *PLoS One*, 2013, vol. 8, no. 11, e79989.
40. Kayser, J., Tenke, C.E., Kroppmann, C.J., et al., Auditory event-related potentials and alpha oscillations in the psychosis prodrome: neuronal generator patterns during a novelty oddball task, *Int. J. Psychophysiol.*, 2014, vol. 91, no. 2, p. 104.
41. Bastiaansen, M. and Hagoort, P., Oscillatory neuronal dynamics during language comprehension, *Prog. Brain Res.*, 2006, vol. 159, p. 179.
42. Kujala, J., Vartiainen, J., Laaksonen, H., and Salmelin, R., Neural interactions at the core of phonological and semantic priming of written words, *Cereb. Cortex*, 2012, vol. 22, no. 10, p. 2305.
43. Mellem, M.S., Bastiaansen, M.C.M., Pilgrim, L.K., et al., Word class and context affect alpha- band oscillatory dynamics in an older population, *Front. Psychol.*, 2012, vol. 3, p. 97.
44. Wang, L., Jensen, O., Brink, D., Weder, N., et al., Beta oscillations relate to the N400m during language comprehension, *Hum. Brain Mapp.*, 2012, vol. 33, no. 12, p. 2898.
45. Brennan, J., Lignos, C., Embick, D., and Roberts, T.P.L., Spectro-temporal correlates of lexical access during auditory lexical decision, *Brain Lang.*, 2014, vol. 133, p. 39.
46. Piai, V., Roelofs, A., and Maris, E., Oscillatory brain responses in spoken word production reflect lexical frequency and sentential constraint, *Neuropsychologia*, 2014, vol. 53, p. 146.

Translated by T. Tkacheva